



FLEXURAL BEHAVIOUR OF RECTANGULAR FRP-TUBES FILLED WITH REINFORCED CONCRETE: EXPERIMENTAL AND ANALYTICAL INVESTIGATIONS

Ahmed Abouzied, PhD
Postdoctoral Fellow, University of Sherbrooke, Canada

Radhouane Masmoudi, PE., PhD
Professor, University of Sherbrooke, Canada

ABSTRACT

This paper presents experimental and analytical investigations on the flexural behaviour of rectangular concrete-filled fiber-reinforced polymer (FRP) tube (CFFT) beams with steel rebar. Eight full-scale CFFT beams and two control reinforced concrete (RC) beams were tested under a four-point bending. Several parameters as the FRP tubes thickness, fiber laminates, and steel reinforcement were studied. The experimental results indicate outstanding performance of the CFFT beams in terms of strength and ductility compared to the RC beams. Some CFFT beams attained flexural strength and ductility 540% and 1430% higher than that of the RC beams, respectively. Theoretical analysis was developed to determine the flexural capacities of the CFFT beam system through cracking, yield, and ultimate stages. A strain compatibility/equilibrium model was developed to predict the moment-curvature response of the CFFT beams addressing the issue of confinement and tension stiffening of concrete. The analytical model can predict well the flexural moments, curvature, deflection, strains, and neutral axis location.

Keywords: Beams, Fiber-Reinforced Polymer, Flexural behaviour, Strain Compatibility, Deflection.

1. INTRODUCTION

Considerable research has been conducted to validate the application of fiber-reinforced polymer (FRP) composites in the construction industry. One of the innovative applications is the concrete-filled FRP tubes (CFFT). Extensive studies have been conducted to investigate the behaviour of CFFTs as columns, but comparatively limited research was carried out on CFFTs as beams especially CFFTs with circular sections. The construction and architectural requirements prefer the rectangular section of beams due to its stability during installation and its workability during connecting to other structural members like slabs and columns. Actually, limited studies have been reported on the flexural behaviour of CFFT beams with rectangular sections (Fam et al. 2005, Belzer et al. 2013). However, none of them reinforced the rectangular CFFT beams with steel rebar or analytically studied the deflection response of the composite section.

The compression failure in most tested circular CFFT beams was predominantly governed by the compression failure of the tube flange under longitudinal compressive stresses where the tensile hoop strains (i.e., confinement effect) were insignificant (AASHTO 2012). This notice is based on flexural tests of circular CFFT beams without steel reinforcement. More investigations are required to verify that notice on rectangular CFFT beams with steel rebar. Unlike steel-or-FRP-RC beams, the steel-reinforced CFFT beams can exhibit superior additional flexural capacities in the post-yielding stage (Abouzied and Masmoudi 2014, 2015). This is attributed to the confining action of the FRP tube on the concrete core to withstand higher strains, and the FRP tube reinforcement contribution in the axial direction, in addition to the reinforcement action of the steel bars in their plastic hardening status. New design equations are required to get benefit of the outstanding flexural capacity at the post-yielding stage, and simultaneously, equations to predict the expected deflection with reasonable accuracy.

Analytical models have been developed to predict the flexural capacity and load-deflection response for circular CFFT beams (Cole and Fam 2006, Fam and Son 2008, Mohamed and Masmoudi 2010). These models are based on strain compatibility, internal forces equilibrium, and material constitutive relationships. The forces within the CFFT cross section were calculated by integrating the stress over the area of each individual material. Despite the limited number of tested specimens, these models predict well the flexural behaviour of their circular CFFT beams. Their theoretical analysis depends mainly on a computer-based analysis and requires some sophisticated calculation procedures. Also, these proposed models require verification and adjustment to be valid for the rectangular CFFT beams, and need to be simplified to be applicable for common designers.

This paper investigates the flexural behaviour of rectangular CFFT beams with steel rebar, particularly in terms of flexural capacities at various stages during the loading, deflection response, and modes of failure, for which very limited published data exist. Also, it attempts to establish a theoretical basis for the development of design procedure inspired by the North American design codes provisions.

2. EXPERIMENTAL PROGRAM

2.1 Materials and Beam Specimens

Five types of rectangular FRP tubes with identical internal cross sections were fabricated at the laboratory of Composites Materials for Infrastructures at Sherbrooke University using the filament-winding process. The FRP tubes were composed of typical E-glass fibers and vinyl-ester resin. The tubes thickness ranged from 3.4 mm to 14.2 mm. The fibers are oriented at different winding angles, 90° , $\pm 30^\circ$, and $\pm 45^\circ$ as shown in Table 1. This orientation aims to increase the flexural strength and stiffness of the FRP tube in the axial direction as well as the transverse direction. Standard tests were carried out to evaluate the physical and mechanical properties of the filament-wound FRP tubes. Tension and compression tests were carried out according to ASTM D3039 (2014) and ASTM D695 (2010), respectively, on identical five coupons to obtain the tensile and compressive strength in each direction. Table 1 lists the detailed physical and mechanical properties of the fabricated FRP tubes. The results of the coupons tests indicate a non-linear behaviour of the FRP composite when increasing the winding angle as shown in Figure 1. The inner surfaces of the tubes were coated by a layer of vinyl-ester resin and coarse sand particles to produce a rough texture in order to enhance the bond between the concrete core and the tubes to achieve a full composite action under flexure.

Ten beams 3200 mm long were fabricated for this study as shown in Table 2; two identical steel-RC beams, two identical CFFT beams of OR2₃₀, OR4₃₀, and OR8₃₀, one beam of OR12₃₀, and one beam of OR16₄₅. All the tested beams were reinforced at the tension side with steel bars 4 Φ 15M. According to the results of a standard tension test ASTM A615 (2009) carried out on three specimens of a steel bar 15M, the average yield tensile strength (f_y) is 467 MPa and the modulus of elasticity E_s is about 200 GPa.

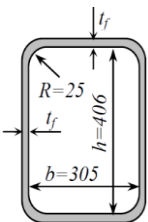
The beams were casted with a ready-mixed normal weight concrete. The RC beams were casted horizontally in a wooden box formwork, while the CFFT beams were fixed on inclined strong frames and the concrete was poured into the tubes from top end gates. The RC beams were cured in a conventional way by spraying water for 7 days. The CFFT beams were covered tightly with plastic sheets and the moisture surrounded the beams was kept at high level for 7 days. After 28 days of casting, concrete cylinders tests were performed according to ASTM C39 (2012). The average unconfined compressive strength for the cylindrical concrete specimens at 28 days old (f'_c) is listed in Table 2.

2.2 Test Setup and Instrumentations

The beams were tested using a four-point bending load setup over a simply supported span of 2920 mm and a distance between the applied concentrated loads of 720 mm centered with the beam as shown in Figure 2. The beams were loaded under displacement control with a rate of 1 mm/min using MTS machine with a capacity of 10000 kN. The beams were unloaded at $0.5\Delta_y$, Δ_y , $2\Delta_y$, and $4\Delta_y$ and then reloaded where Δ_y is a pre-calculated deflection at yielding of the steel rebar. The unloading and reloading scheme was intended for the assessment of stiffness at various load levels and to evaluate the ductility of such beam system.

Three displacement potentiometers (DPs) were used to monitor the deflection profile along the beam span, whereas another two DPs were located at the ends of the beams to record any relative displacement (slip) between the concrete core and the tube. Electrical strain gages were bonded on the steel reinforcing bars before casting at the most critical section at mid-span. In addition, axial and transverse strain gages were bonded directly on the tubes surfaces at different levels along the beams depth to record the strains and the confining action around the section. Additional Linear variable differential transducers (LVDTs) were affixed at the beams top and bottom faces to monitor the extreme axial compressive and tensile strains. Strain rosettes were located at the center of the shear span to investigate the shear response of the beams. The load, deflection, and strains were recorded during the tests using a data acquisition system.

Table 1: GFRP tubes configurations and mechanical properties

Tube	Cross Section (mm)	Stacking sequence	% Fibers	t_f (mm)	Mechanical properties	Axial direction			Transverse direction		
						E_{lo} (GPa)	F_{lo} (Mpa)	ϵ_{lo} (mm/m)	E_{tr} (Gpa)	F_{tr} (Mpa)	ϵ_{tr} (mm/m)
OR2 ₃₀		[90°, ±30°, 90°]	62	3.4	Ten. Test	14.3±2	158±20	15.7±5	16.0±1	257±26	21.8±2
					Comp. test	14.0±3	-92±9	-7.0±1	17.8±2	-175±9	-10.4±1
OR4 ₃₀		[90°, ±30°, 90°, ±30°, 90°]	61	5.7	Ten. Test	14.5±1	173±9	15.3±2	14.4±1	249±25	23.9±3
					Comp. test	15.5±1	-165±7	-12.5±1	14.5±1	-293±18	-24.0±3
OR8 ₃₀		[90°, ±30°, 90°, ±30°, 90°]	59	8.7	Ten. Test	16.2±1	197±16	18.9±2	13.7±1	168±6	19.2±1
				Comp. test	17.7±1	-189±9	-11.8±1	13.8±1	-211±13	-17.8±1	
OR12 ₃₀	[90°, ±30°, 90°, ±30°, 90°]	59	9.9	Ten. Test	18.6±1	242±13	15.3±1	13.4±1	125±9	16.6±2	
				Comp. test	20.1±2	-176±12	-9.5±1	12.2±1	-217±16	-24.0±3	
OR16 ₄₅	[90°, ±45°, 90°, ±45°, 90°]	58	14.2	Ten. Test	10.5±2	100±14	22.7±6	13.0±1	164±3	24.5±2	
				Comp. test	11.1±1	-110±6	-20.7±1	12.2±1	-171±7	-21.4±2	

E , F , and ϵ are the elasticity modulus, stress, and strain, respectively.

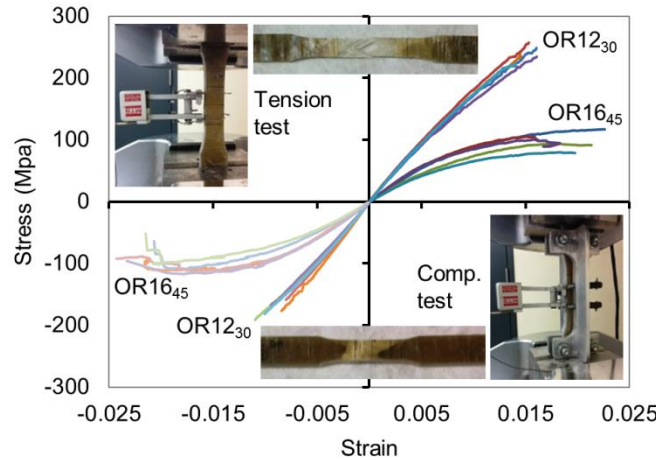


Figure 1: Typical coupons test results in the axial direction

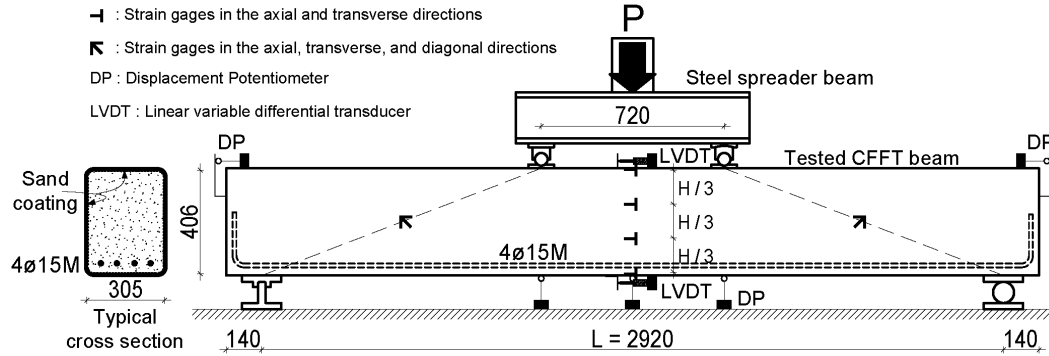


Figure 2: Schematic of test setup (Dimensions are in mm)

Table 2: Beam specimens and summary of test results

Group	Beam ID	Section shape (mm)	Steel reinforcement	Outer tube	Concrete strength (MPa)	Moment (kN.m)			Ultimate Deflection (mm)	Ductility (kN.m ²)	Failure mode
						M_{cr}	M_y	M_u			
RC beams	RC #1		Top 2Φ10M Bot. 4Φ15M	---	41.7	30	113	132	29	3.1	Tension
	RC #2		Ties Φ10M/150 mm			31	116	130	29	3.1	Tension
CFFT beams	OR2 ₃₀ #1		Bot. 4Φ15M	OR2 ₃₀	49.7	43	152	249	52	10.2	Tension
	OR2 ₃₀ #2				43	150	267	69	14.3	Tension	
	OR4 ₃₀ #1			OR4 ₃₀	48.7	46	161	404	89	27.0	Tension
	OR4 ₃₀ #2				44	168	392	77	22.2	Tension	
	OR8 ₃₀ #1			OR8 ₃₀	41.7	48	204	559	82	33.0	Balanced
	OR8 ₃₀ #2				45	210	560	92	38.4	Balanced	
	OR12 ₃₀			OR12 ₃₀	48.7	50	245	581	45	17.5	Comp.
	OR16 ₄₅			OR16 ₄₅	48.7	50	235	712	97	47.5	Balanced

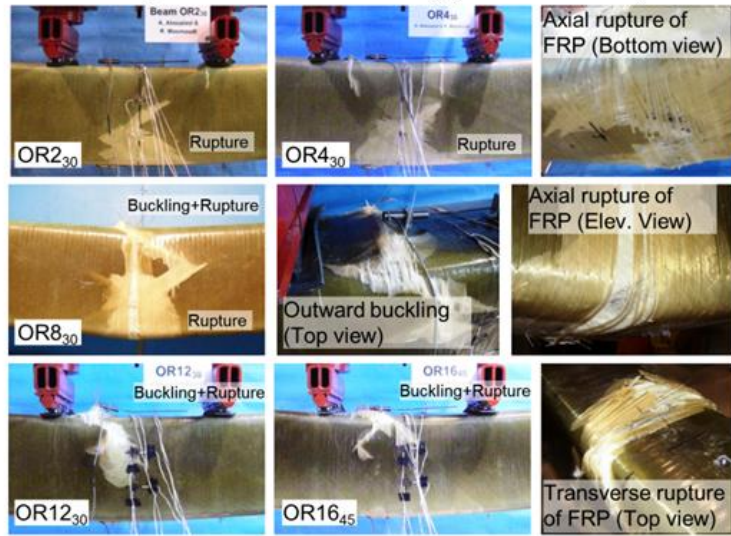
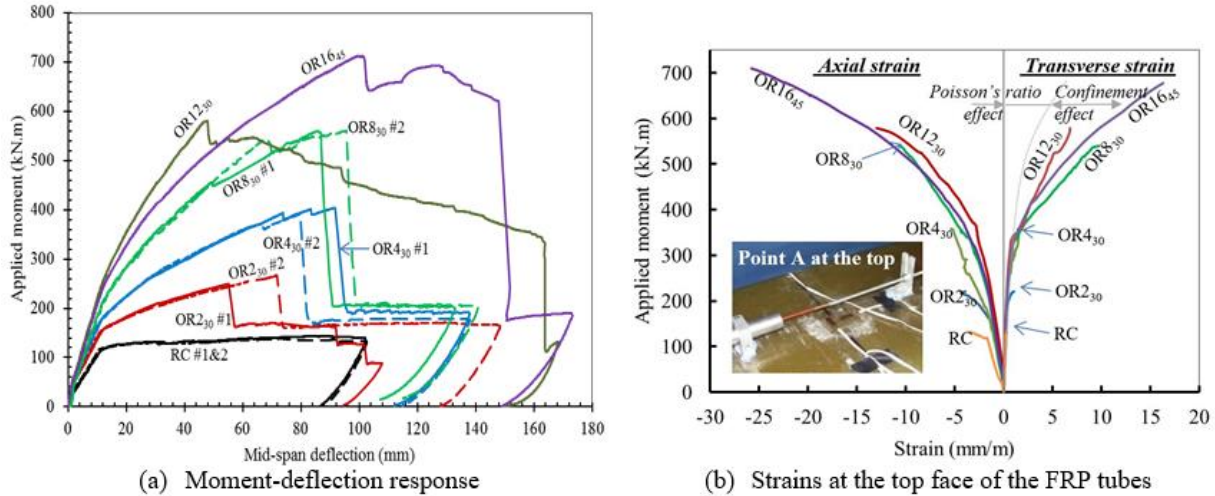
3. TEST RESULTS

3.1 Flexural Behaviour of Rectangular CFFT Beams

All the beams failed under flexure without any signs of shear failure, slip, or web buckling. The cyclic loading did not affect the load-deflection response since the maximum gap in the deflection within the cycles did not exceed 1 mm until the peak load. This is attributed to the elastic behavior of this type of hybrid CFFT beams. Figure 3 shows the typical failure patterns of the CFFT beams and their moment-deflection responses (outer envelopes) in addition to the strains at the top face of the FRP tubes. OR2₃₀ with FRP tube thickness of 3.4 mm failed in tension with axial rupture of fibers at the tension side. Also, OR4₃₀ with FRP tube thickness of 5.7 mm experienced a tension failure however there was inflate and minor signs of outward buckling at the top flange before the ultimate failure. The failure of OR8₃₀ with FRP tube thickness of 8.7 mm started with outward buckling of the tube compression flange with a limited drop in strength. Accordingly, the flexural stiffness decreased. Nevertheless, the tube continued to carry additional loads depending mainly on the tube bottom flange at the tension side and the confined concrete at the compression side. Shortly thereafter, an axial rupture of fibers at the tension side happened. OR12₃₀ with FRP tube thickness of 9.9 mm failed in compression by outward buckling of the compressive flange with a limited loss of strength, but the beam could not carry any additional loads afterwards. OR16₄₅ with FRP tube thickness of 14.2 mm behaved in the same way as OR8₃₀. Note that, OR16₄₅ experienced the maximum flexural capacity due to its high resistance to buckling. This is attributed to the high percentage of the transverse fibers in OR16₄₅ that resisted the

buckling of the axial fibers unlike the case in OR12₃₀. Accordingly, the buckling of the tube compression flange affected the flexural capacity of OR12₃₀. Figure 3(b) shows that the confinement efficiency appear in the thick tubes (OR8₃₀, OR12₃₀, and OR16₄₅) more than the thin tubes (OR2₃₀ and OR4₃₀). This confirms the transverse rupture of fibers at the top face of OR16₄₅ shown in Figure 3(c). Based on the noticed patterns of failure of the tested CFFT beams, OR2₃₀ and OR4₃₀ could be considered as under-reinforced CFFT beam sections, while OR12₃₀ could be considered as over-reinforced CFFT beam sections, while OR8₃₀ and OR16₄₅ could be considered as balanced CFFT beam sections as listed in Table 2. Even after the ultimate failure, the reinforced CFFT beams kept a residual strength due to the existence of the steel that has a high plastic strain (see the horizontal yielding plateau after the ultimate failure in Figure 3(a)), unlike the FRP-concrete composite beams that commonly lose their flexural strength entirely once their FRP reinforcement fails.

The overall moment-deflection behaviour of the rectangular CFFT beams reinforced with steel rebar is non-linear. The flexural stiffness was very high before cracking due to the high value of the gross moment of inertia (I_g) and then it decreased after cracking of the concrete. The flexural stiffness decreased more after yielding of the steel, but there was an ascending flexural capacity that cannot be neglected as in the RC beams. The results indicate also the significant gain in strength, stiffness, and ductility of the rectangular CFFT beams compared to the RC beam. The ductility of the beams were indicated by the energy absorption determined by the area under the moment-deflection curves until the peak capacity as listed in Table 2. The results indicate that the ductility of the CFFT beams attained values 1430% greater than that of the RC beam as in OR16₄₅. The moment at the yield of steel (M_y) of the CFFT beams is also greater than that of the RC beams, and increases with increasing the FRP tube contribution by its thickness and/or axial strength. For example, M_y of the CFFT beams OR2₃₀ with 3.4 mm tube thickness is 32% higher than that of the RC beams. While M_y of the CFFT beam OR12₃₀ with 9.9 mm tube thickness is 114% higher than that of the RC beams. The ultimate flexural capacity (M_u) of the CFFT beams attained value 540% higher than that of the RC beam as in OR16₄₅.



(c) Failure patterns
Figure 3: Beam test results

3.2 Cracking Strength in CFFT Beams

One of the advantages of the CFFT system is that the outer FRP tube acts as a jacket that protects the inner structural elements, such as concrete and steel, against corrosion even if the inner concrete core is cracked. It is important for effective design of FRP-concrete composite structure to study the cracking behaviour for serviceability requirements related to deflection and crack width control. Although the concrete core was hidden behind the tubes surface, the moment at the first crack (M_{cr}) was obtained from the readings of the steel strains and the curvature response change. In this study, the experimental M_{cr} and the moment of inertia of the gross transformed section (I_g) were used to develop an expression for the modulus of rupture of concrete (f_{cr}) using the following equations:

$$[1] \quad f_{cr} = M_{cr} Y_t / I_g = k \sqrt{f'_c}$$

$$[2] \quad I_g = I_c + (n_s - 1) I_s + n_f I_f$$

Where I_c , I_s , and I_f are the moment of inertia of the concrete, steel bars, and FRP tube, respectively. Y_t is the distance of the extreme tension fiber of concrete from the centroid. n_s is the steel modular ratio ($n_s = E_s / E_{co}$). n_f is the FRP

modular ratio ($n_f = E_f/E_{co}$). E_f is the elasticity modulus of the FRP tube approximated as the average of the axial elasticity modulus in tension and compression. E_{co} is the elasticity modulus of the concrete ($E_{co}=4500\sqrt{f'_c}$).

Based on this study, the coefficient $k = 0.69$ in case of calculating I_g considering reinforcement (FRP tube + steel) and $k = 0.8$ in case of calculating I_g neglecting reinforcement. Note that, ACI-318 (2014) uses $k = 0.62$ and recommends neglecting reinforcement in calculating I_g . By comparing the k values of the current study and ACI-318, it can be seen that the cracking strength can be increased by 30% in the CFFT beams. It is attributed to many factors:

1. The FRP tubes contributed positively in the gross section inertia I_g .
2. The bond between the FRP tubes surfaces and the concrete delayed the generation of the cracks.
3. Confining the concrete with FRP tubes restrained it against cracks propagation.
4. The concrete expansion during curing was restrained by the tube inducing chemical pre-stressing on the concrete (Fam and Rizkalla 2002).

3.3 Yield and Ultimate Moments

An analytical model based on strain compatibility/equilibrium was developed to predict theoretically the flexural capacity of rectangular CFFT beams as shown in Figure 4(a). The model is based on the assumption that plain sections remain plain after deformation, which means linear strain distribution along the depth of the CFFT section subjected to bending. This model assumes also full bond between the concrete core, steel bars, and the FRP tubes (no slip). By assuming the depth of the compression zone (c) and the strains at any level (steel level or tube top and bottom faces), the internal tension and compression forces along the cross section can be determined as shown in Table 3.

The parts of the rectangular FRP tube above and below the neutral axis were considered effective in resisting the compression and tension forces, respectively. A linear stress-strain relationship was assumed for the FRP with maximum limits for strength and strains obtained from coupon tests results (See Table 1). Therefore, Secant's moduli are used to model the FRP tube in tension and compression as $E_{ten}=F_{lo(ten)}/\epsilon_{lo(ten)}$ and $E_{comp}=F_{lo(comp)}/\epsilon_{lo(comp)}$, respectively.

The steel was modeled by a bilinear model in two parts: (1) a linear elastic part up to the yield strain ($\epsilon_s = f_y/E_s = 0.0023$), (2) a yield plateau up to the ultimate plastic strain with a zero plastic hardening elasticity modulus. Two models for concrete in compression are examined in this study as shown in Figure 4(b). The first concrete model is an unconfined concrete model with extended strain softening using Popovics's model (1973) as suggested by AASHTO guidelines (2012) and shown in Eq. 3.

$$[3] \quad f_c = \frac{f'_c(\epsilon_c/\epsilon'_c)^r}{r-1+(\epsilon_c/\epsilon'_c)^r} \quad \text{and} \quad r = E_{co}/(E_{co} - E_{sec})$$

Where, the secant modulus of concrete $E_{sec} = f'_c/\epsilon'_c$ and the maximum compressive strain $\epsilon'_c = 0.002$ based on the compressed cylinder test results.

The second concrete model is a partially confined concrete model, which is based on a function similar to the Popovics's model up to f'_c followed by plastic behaviour with constant compressive strength equals f'_c as shown in Figure 4(b). This model was chosen to present intermediate level of confinement that is adequate for beams, instead of full confinement models that are adequate for columns.

The tensile strength and tension stiffening of concrete in tension are also considered in the model as shown in Figure 4(b). The maximum tensile strength of concrete $f_{cr} = 0.62\sqrt{f'_c}$ and the corresponding tensile strain $\epsilon_{cr} = f_{cr}/E_{co}$. For $\epsilon_c \geq \epsilon_{cr}$, the concrete tension stiffening model proposed by Collins and Mitchell (1997) was used as follows:

$$[4] \quad f_c = \frac{\alpha_1 \alpha_2 f_{cr}}{1 + \sqrt{500(\epsilon_c - \epsilon_{cr})}}$$

Where, α_2 is a factor accounting for the nature of loading and was taken as 0.7 for repeated loading. α_1 is a factor accounting for the bond characteristics and was taken as 1.0 because of the full composite action.

Due to the non-linearity of the concrete material, the concrete parts above and below the neutral axis are divided into n number of strips, which have the same thickness h_i . Where $h_i = c / n$ for the strips in the compression zone and $h_i = (h - c)/n$ for the strips in the tension zone. The centroid of each strip, i , is located at its mid-thickness. The distance from each compression strip centroid to the neutral axis, YC_i , and the strain ε_{ci} at its mid-thickness are calculated from Eq. 5. The distance from each tension strip centroid to the neutral axis, YT_i , and the strain ε_{ti} at its mid-thickness are calculated from Eq. 6.

$$[5] \quad YC_i = \frac{c}{n}(i - 0.5) \rightarrow \varepsilon_{ci} = \varepsilon_{cc} \frac{YC_i}{c} \dots \text{For strips in the compression zone}$$

$$[6] \quad YT_i = \frac{h-c}{n}(i - 0.5) \rightarrow \varepsilon_{ti} = \varepsilon_{ct} \frac{YT_i}{h-c} \dots \text{For strips in the tension zone}$$

These strain values are retrieved in Eq. 3 and Eq. 4 to obtain the corresponding compressive stress or tensile stress in concrete, respectively. Then, the internal compression or tension force, C_{ci} or T_{ci} , inside each strip is calculated as:

$$[7] \quad C_i = f_{ci} b h_i \dots (f_{ci} \text{ from Eq. 3})$$

$$[8] \quad T_i = f_{ti} b h_i \dots (f_{ti} \text{ from Eq. 4})$$

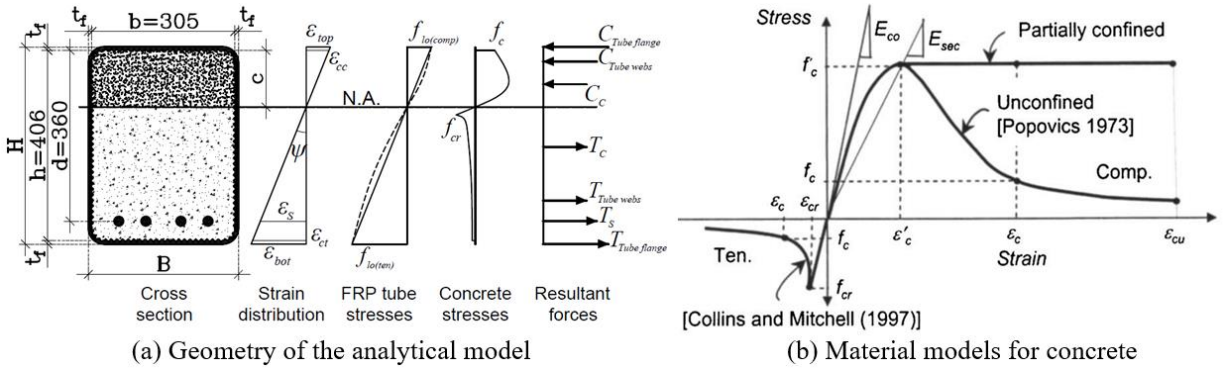


Figure 4: Analytical model

Table 3: The internal forces and their positions in rectangular CFFT beams

Internal Force ID	Expression of the force	Distance from the neutral axis
Tension force in steel	$T_s = E_s \cdot \varepsilon_s \cdot A_s \leq f_y \cdot A_s$	$YT_s = d - c$
Tension force in tube flange	$T_{Tube\ flange} = b t_f E_{ten} \left(\frac{\varepsilon_{bot} + \varepsilon_{ct}}{2} \right)$	$YT_{Tube\ flange} = h - c + \frac{t_f}{2}$
Tension force in tube webs	$T_{Tube\ webs} = (h - c) t_f E_{ten} \varepsilon_{ct}$	$YT_{Tube\ webs} = \frac{2}{3}(h - c)$
Tension force in concrete strips	$T_i = f_{ci} b h_i \rightarrow T_c = \sum_{i=1}^{i=n} T_i$	$YT_i = \frac{h-c}{n}(i - 0.5)$
Compression force in tube flange	$C_{Tube\ flange} = b t_f E_{comp} \left(\frac{\varepsilon_{cc} + \varepsilon_{top}}{2} \right)$	$YC_{Tube\ flange} = c + \frac{t_f}{2}$
Compression force in tube two webs	$C_{Tube\ webs} = c t_f E_{comp} \varepsilon_{cc}$	$YC_{Tube\ webs} = \frac{2c}{3}$
Compression force in concrete strips	$C_i = f_{ci} b h_i \rightarrow C_c = \sum_{i=1}^{i=n} C_i$	$YC_i = \frac{c}{n}(i - 0.5)$

3.4 Procedure of Analysis

1. Specify the tube dimensions, thickness, material properties, location and area of steel rebar, and number of concrete strips, n .
2. Assume a strain value, i.e., $\varepsilon_s = F_y/E_s$ if M_y is required or $\varepsilon_{bot} = \varepsilon_{lo(ten)}$ if M_u is required.
3. Assume a value for the compression zone depth c .
4. Calculate the strains at different levels, i.e., the strain at steel rebar (ε_s), the strain at the top face of the FRP tube (ε_{top}), the strain at top face of concrete (ε_{cc}), the strain at the bottom face of concrete (ε_{ct}), and the strain at the bottom face of the FRP tube (ε_{bot}).
5. For each concrete strip in compression and tension, compute the strains at its mid-thickness (ε_{ci} or ε_{ti}) and the corresponding compressive or tensile stresses.
6. Calculate the total compressive and tensile forces in the concrete, rebar, and the FRP tube.
7. Check for equilibrium by satisfying $\Sigma C = \Sigma T$ with allowable tolerance.
8. If the equilibrium is not satisfied, go to step 3 and assume another value for c . The process is repeated until the equilibrium is satisfied.
9. Once the equilibrium is satisfied, the internal moments are calculated for all the internal forces around the neutral axis as $M_{theo} = \Sigma(F_i Y_i)$, and the corresponding curvature is calculated as $\psi = \varepsilon_{top} / (c + t_f)$.

The previous steps can be repeated many time by assuming sequential values of strains from zero to maximum coupons strains in order to construct moment-curvature response. Once the curvature is obtained, the deflection (Δ) of a four-point loading system can be estimated from corresponding curvatures at any level (service load or ultimate load) by Eq. 9 where L is the span between the supports and a is the shear span.

$$[9] \quad \Delta = \frac{\psi}{24} (3L^2 - 4a^2)$$

3.5 Analytical Results

Two typical examples for CFFT beams with thin FRP tube and thick FRP tubes are shown in Figure 5 which plots the effect of using the unconfined-or-confined concrete models on the neutral axis location and corresponding moments. The partially confined concrete model indicates good prediction for the flexural behaviour of all tested CFFT beams. While the unconfined concrete model can be used in the FRP tubes that have small tube thickness only. For example in the CFFT beam OR2₃₀, the response of the unconfined and confined concrete model was identical until the ultimate predicted moment. While in the CFFT beam OR12₃₀, the response that uses the unconfined concrete model was not able at all to predict well their flexural response and deviates from the experimental results at about 60% of the ultimate moments. Accordingly, the unconfined concrete model is conservative especially in the thick tubes. These theoretical results match well with the experimental results indicated in Figure 3(b) that indicates confinement presence in the CFFT beams with thick FRP tubes unlike the CFFT beams with thin FRP tubes.

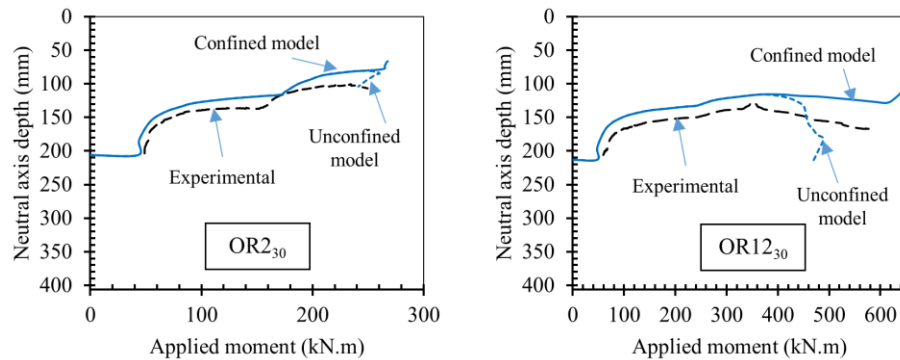


Figure 5: Effect of concrete confinement model

Until yield, both unconfined and confined concrete models give the same results since the confinement has not been activated yet ($\varepsilon_{top} < \varepsilon'_c$ as shown in Table 4). Table 4 lists the predicted versus experimental yield moments of the CFFT beams and the tension stiffening of the concrete is considered or ignored. The results indicate that the tension

stiffening can be considered in the thick tubes and should be ignored in the thin tubes to match well the experimental results. It is attributed to, the thick tubes confine well the inner concrete core and prevent it from excessive cracks unlike the thin tubes. Nevertheless, ignoring the tension stiffening of concrete underestimates the experimental results and achieves safe design. The same observation can be seen in Table 5 that lists the predicted versus experimental ultimate moments of the CFFT beams. The analytical results justify the use of the partially confined concrete model in modelling the rectangular CFFT beams. Figure 6 shows the experimental versus the analytical results of moment-deflection responses for two examples of the tested CFFT beams using the partially confined concrete model. Good agreement is observed, however in CFFT beams with thin FRP tubes, ignoring the tension stiffening shows better agreement with the experimental profiles of deflection than considering it.

Table 4: Theoretical versus experimental yield moments

CFFT Beam	$M_y(\text{exp.})$ (kN.m)	ϵ_s (mm/m)	Unconfined or partially confined concrete model									
			Considering tension stiffening					Ignoring tension stiffening				
			ϵ_{top} (mm/m)	ϵ_{bot} (mm/m)	c (mm)	$M_y(\text{th.})$ (kN.m)	$\frac{M_y(\text{exp.})}{M_y(\text{th.})}$	ϵ_{top} (mm/m)	ϵ_{bot} (mm/m)	c (mm)	$M_y(\text{th.})$ (kN.m)	$\frac{M_y(\text{exp.})}{M_y(\text{th.})}$
OR2 ₃₀ #1	152	2.3	1.1	2.8	113	171	0.89	1.0	3.2	95	149	1.02
OR2 ₃₀ #2	150		1.1	2.8	113	171	0.88	1.0	3.2	95	149	1.01
OR4 ₃₀ #1	161		1.2	2.8	117	189	0.85	1.0	2.8	105	161	1.00
OR4 ₃₀ #2	168		1.2	2.8	117	189	0.89	1.0	2.8	105	161	1.04
OR8 ₃₀ #1	204		1.3	2.8	123	206	0.99	1.1	2.8	110	188	1.08
OR8 ₃₀ #2	210		1.3	2.8	123	206	1.02	1.1	2.8	110	188	1.12
OR12 ₃₀	245		1.3	2.9	123	239	1.03	1.2	2.9	114	215	1.14
OR16 ₄₅	235		1.3	2.9	122	223	1.05	1.2	2.8	112	201	1.17

Table 5: Theoretical versus experimental ultimate moments

CFFT Beam	$M_u(\text{exp.})$ (kN.m)	Partially confined concrete model									
		Considering tension stiffening					Ignoring tension stiffening				
		ϵ_{top} (mm/m)	ϵ_{bot} (mm/m)	c (mm)	$M_u(\text{th.})$ (kN.m)	$\frac{M_u(\text{exp.})}{M_u(\text{th.})}$	ϵ_{top} (mm/m)	ϵ_{bot} (mm/m)	c (mm)	$M_u(\text{th.})$ (kN.m)	$\frac{M_u(\text{exp.})}{M_u(\text{th.})}$
OR2 ₃₀ #1	249	3.5	15.2	74	265	0.94	3.0	15.9	62	239	1.04
OR2 ₃₀ #2	267	3.5	15.2	74	265	1.01	3.0	15.9	62	239	1.12
OR4 ₃₀ #1	404	4.5	15.5	88	359	1.13	4.0	15.9	78	336	1.20
OR4 ₃₀ #2	392	4.5	15.5	88	359	1.09	4.0	15.9	78	336	1.17
OR8 ₃₀ #1	559	7.0	18.0	110	498	1.12	7.0	20.5	100	488	1.15
OR8 ₃₀ #2	560	7.0	18.0	110	498	1.12	7.0	20.5	100	488	1.15
OR12 ₃₀	581	8.0	15.1	118	615	0.94	6.0	15.3	110	589	0.99
OR16 ₄₅	712	7.0	22.5	121	601	1.18	6.0	23.0	113	575	1.24

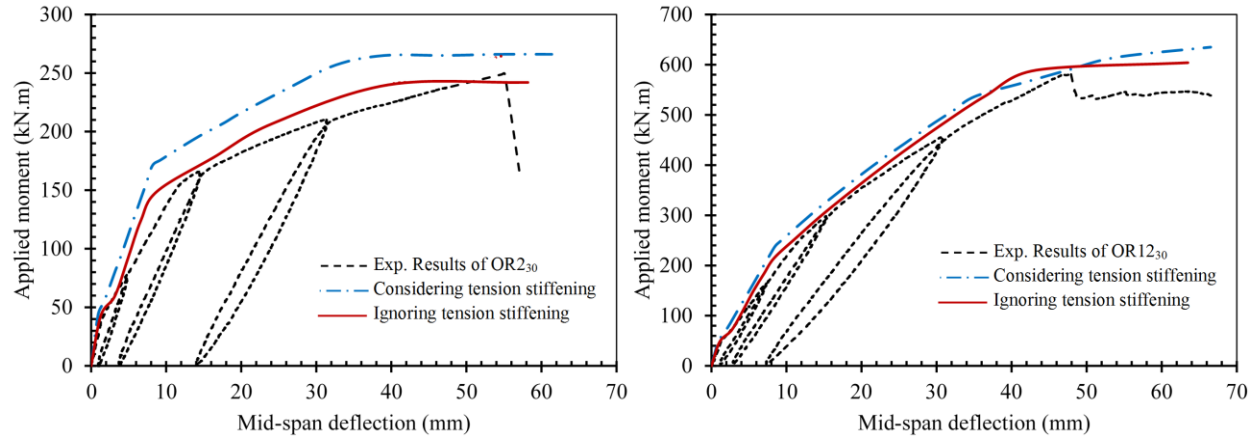


Figure 6: Theoretical versus experimental moment deflection response of CFFT beams

4. CONCLUSIONS

The main concluded points of this study are as following:

1. The rectangular CFFT beams experience significantly higher ductility, higher stiffness, and superior strength than the RC beams.
2. The rectangular CFFT beams with steel rebar fail gradually in a sequential manner (yielding of steel, buckling of compressed tube flange, and finally rupture of the fibers). Even after the ultimate failure, the steel reinforced CFFT beams keep a residual strength because of the existence of the steel that withstands high strains and elongation.
3. The reinforced CFFT rectangular beams experience high cracking strength and the concrete modulus of rupture (f_{cr}) suggested by ACI-318 could be increased by 30% if the gross moment of inertia I_g is calculated neglecting reinforcement.
4. The analytical model proposed in this study is capable of predicting well the moment-curvature, moment strains, neutral axis depth, and moment-deflection responses of fully-CFFT rectangular beams. The confinement and tension stiffening issues of concrete are considered in the model.
5. Using partially confined model for concrete with plastic strain up to the ultimate compressive strain of the FRP tube material indicate better agreement with the experimental results than using the unconfined concrete model proposed by AASHTO guidelines (2012).
6. Concrete tension stiffening can be considered in CFFT beams with thick tubes, and should be ignored in CFFT beams with thin tubes.

ACKNOWLEDGMENTS

The research reported in this paper was partially sponsored by the Natural Sciences and Engineering Research Council of Canada (NSERC) and the 'Fonds de recherche québécois-Nature et Technologie'. The authors also acknowledge the contribution of the Canadian Foundation for Innovation (CFI) for the infrastructure used to conduct testing. The opinion and analysis presented in this paper are those of the authors.

REFERENCES

- AASHTO. Guide specifications for design of concrete-filled FRP tubes for flexural and axial members. 1st edition, Washington, DC; 2012.
- Abouzied, A. and Masmoudi, R. 2014. Flexural behaviour of new partially concrete-filled filament-wound rectangular FRP tube beams. *4th international structural specialty conference CSCE*, Halifax, NS, Canada, 10 p. paper in CD-ROM proceedings.

- Abouzied, A. and Masmoudi, R. 2015. Structural performance of new fully and partially concrete-filled rectangular FRP-tube beams. *Construction and Building Materials Journal*, 101: 652-660.
- American Concrete Institute. 2014. Building code requirements for structural concrete. ACI 318-14. Detroit, USA.
- ASTM. 2009. Standard specification for deformed and plain carbon steel bars for concrete reinforcement. ASTM A615/A615M. West Conshohocken, PA.
- ASTM. 2010. Standard test method for compressive properties of rigid plastics. ASTM D695. West Conshohocken, PA.
- ASTM. 2012. Standard test method for compressive strength of cylindrical concrete specimens. ASTM C39. West Conshohocken, PA.
- ASTM. 2014. Standard test method for tensile properties of polymer matrix composite materials. ASTM D3039/D3039M. West Conshohocken, PA.
- Belzer, B., Robinson, M., and Fick, D. 2013. Composite action of concrete-filled rectangular GFRP tubes. *ASCE Composites for Construction Journal*, 17(5): 722-731.
- Cole, B. and Fam, A. 2006. Flexural load testing of concrete-filled FRP tubes with longitudinal steel and FRP rebar. *ASCE Composites for Construction Journal*, 10(2): 161-171.
- Collins, M. P. and Mitchell, D. 1997. Prestressed concrete structures. Response Publications, Canada.
- Fam, A. and Rizkalla, S. 2002. Flexural behaviour of concrete-filled fiber-reinforced polymer circular tubes. *ASCE Composites for Construction Journal*, 6(2): 123-132.
- Fam, A. and Son, J. K. 2008. Finite element modeling of hollow and concrete-filled fiber composite tubes in flexure: optimization of partial filling and a design method for poles. *Engineering Structures Journal*, 30: 2667-2676.
- Fam, A., Schnerch, D., and Rizkalla, S. 2005. Rectangular filament-wound glass fiber reinforced polymer tubes filled with concrete under flexural and axial loading: experimental investigation. *ASCE Composites for Construction Journal*, 9: 25-33.
- Mohamed, H. and Masmoudi, R. 2010. Flexural strength and behaviour of steel and FRP-reinforced concrete-filled FRP tube beams. *Engineering Structures Journal*, 32: 3789-3800.
- Popovics, S. 1973. A numerical approach to the complete stress-strain curve of concrete. *Cement and Concrete Research Journal*, 3(5): 583-599.